

HEAT TRANSFER ENHANCEMENT USING VORTEX PROMOTERS IN MAGNETO-HYDRO-DYNAMIC FLOWS

Oliver. G. W. CASSELLS^{*}, Wisam K. HUSSAM and Gregory J. SHEARD

Department of Mechanical and Aerospace Engineering, Monash University, Victoria 3800, AUSTRALIA

^{*}Corresponding author, E-mail address: oliver.cassells@monash.edu

ABSTRACT

The effect of vortex promoter orientation on heat transfer enhancement from a duct side-wall in which an electrically conducting fluid flows under the influence of a transverse magnetic field is investigated. A quasi-two-dimensional magneto-hydrodynamic model is employed to model the flow using high resolution numerical simulation. The gap height and angle of attack of a cylinder with rectangular cross-section (aspect ratio $\alpha = 1/2$) and blockage ratio $\beta = 1/4$, were independently varied to establish relationships between obstacle configuration and heat transfer efficiency. The heat transfer efficiency is measured through an efficiency index defined by the ratio of heat transfer enhancement to pressure drop penalty in comparison to an empty duct case. At gap height ratios $1.15 \leq G/L_c < 2$ for an upright cylinder above a heated lower wall, thermal enhancement and efficiency can be improved, with a peak thermal efficiency of $\eta = 1.6$ occurring at $G/L_c = 1.5$. For a cylinder offset at $G/L_c = 1.5$, varying the incidence angle through $-37.5^\circ < \gamma \leq 22.5^\circ$, $-7.5^\circ < \gamma < 0^\circ$ and $0^\circ < \gamma \leq 15^\circ$ can lead to additional thermal efficiency benefits, with a global peak efficiency of $\eta = 1.7$ occurring at $\gamma = -37.5^\circ$.

NOMENCLATURE

a duct depth (out-of-plane)
 B uniform magnetic field strength
 G gap between cylinder centroid and heated duct wall
 h duct height (y -direction)
 h_c cylinder reference height
 Ha Hartmann number
 L length of duct (x -direction)
 L_c cylinder reference length
 L_d downstream length of duct (from cylinder centroid)
 L_u upstream length of duct (from cylinder centroid)
 N_p polynomial mapping function order
 Nu time averaged Nusselt number
 Nu_w local Nusselt number along heated side-wall
 p kinematic pressure
 Pe Peclet number
 Re Reynolds number (based on L_c)
 Re_m magnetic Reynolds number
 t time
 T temperature
 T_f bulk fluid temperature
 T_o cold wall and fluid temperature
 T_w hot wall temperature
 \mathbf{u} quasi-two-dimensional velocity vector
 U_o peak velocity at duct inlet
 x stream-wise direction Cartesian coordinate

y transverse direction Cartesian coordinate
 z vertical out-of-plane Cartesian coordinate
 α cylinder aspect ratio
 β blockage ratio
 γ incidence angle
 δ_s Shercliff layer thickness
 ΔP total pressure drop across the duct
 Δt time step size (numerical integration time)
 η efficiency index
 ν fluid kinematic viscosity
 ρ fluid density
 σ electrical conductivity
 ω Fourier spectra frequency

INTRODUCTION

The primary motivation for this research is the optimization of heat transfer enhancement through flow disturbance in magneto-hydro-dynamic (MHD) flows occurring in the liquid metal cooling blankets surrounding magnetically confined fusion reactor plasma. Liquid metals moving under the influence of magnetic fields are subjected to electro-magnetic 'Lorentz' forces due to interactions with motion-induced electric currents (Sommeria and Moreau 1982). Research has shown that for sufficiently strong transverse magnetic fields, velocity differentials in perpendicular planes are strongly suppressed, while vortices also become elongated and aligned with the magnetic field (Sommeria and Moreau 1982). Duct walls normal to the magnetic field are subjected to the formation of boundary layers, known as Hartmann layers, which exert frictional forces on the internal core flow. For heat intensive applications, such as fusion reactor cooling blankets, this suppression of turbulent structures is detrimental to the operational efficiency; where the removal of large amounts of thermal energy is required.

A quasi-two-dimensional (Q2D) model can be constructed to investigate these flows by augmenting the two-dimensional Navier-Stokes equations with additional forcing and linear braking terms, representing the Lorentz forces and friction in the Hartmann layers, respectively (Poth erat et al. 2000). The conditions under which the Q2D model remains valid will not be discussed in the present paper for brevity. However, the reader is encouraged to refer to works such as Poth erat et al. (2000), Hussam and Sheard (2013), and Kanaris et al. (2013) for discussion of the validity criteria.

Heat transfer characteristics using internal obstacles to induce transverse vortices in MHD flows has been the

subject of investigation of numerous studies (Yoon et al. 2004, Hussam et al. 2012, Hussam and Sheard 2013, Chatterjee and Gupta 2015). However, only a few studies have investigated the variation of geometric parameters in MHD channel flow on heat transfer characteristics (Branover et al. 1995, Hussam and Sheard 2013). Most pertinent to the methodology of the current study, Hussam and Sheard (2013) showed that there is an optimal gap height above a heated wall at which a circular cylinder should be placed to maximise heat transfer efficiency for certain blockage ratios ($\beta < 1/3$). This optimal spacing was between approximately 1 and 1.5 times the characteristic length of the obstacle. At this location, wake vortices are cast close enough to the heated wall to enhance mixing between low and high temperature fluids, but are still cast high enough to prevent vortex suppression due to interaction with the Shercliff layers. With respect to hydrodynamics research, Meis et al. (2010) numerically investigated the effect of vortex promoter shape, angle of attack, aspect ratio and blockage ratio for low Re two-dimensional hydrodynamic flows on the heat transfer characteristics from a heated lower wall. Thermal efficiency improvement was found to be more strongly dependent on incidence angle than on position relative to the channel centre-line. On the balance of manufacturability and performance, they concluded that an inclined rectangular vortex promoter with aspect ratio $\alpha = 1/2$ would be effective for heat intensive applications. It is therefore expected that there is some finite gap height ratio and incidence angle that maximise the heat transfer efficiency for quasi-two-dimensional MHD duct flow.

The present work aims to identify the optimal heat transfer efficiency configurations by varying gap height and incidence angle of rectangular vortex generators with $\alpha = 1/2$ and $\beta = 1/4$ in quasi-two-dimensional MHD duct flow for $Re = 2000$ and $Ha = 200$.

METHODOLOGY

Problem Definition

The system under consideration is shown in Fig.1. An electrically and thermally insulated rectangular cylinder with cross-section aspect ratio $\alpha = h_c/L_c = 1/2$ and blockage ratio $\beta = L_c/h = 1/4$ orientated with its axis perpendicular to the flow direction and parallel to the magnetic field vector B is confined in a long rectangular duct of length $L = 50L_c$ with out-of-plane depth $a = 2L_c$. The electrically insulated upper and lower duct walls are kept at representative cold and hot temperatures T_o and T_w , respectively. A homogeneous magnetic field of magnitude B acts parallel to the cylinder axis. The upstream and downstream lengths in relation to the vortex promoter centroid are $L_u = 15L_c$ and $L_d = 35L_c$, respectively. The effect of gap height ratio G/L_c of a single upright cylinder for $0.8 \leq G/L_c \leq 3.2$ on heat transfer efficiency is firstly considered. The influence of cylinder incidence angle γ on heat transfer efficiency at the optimal efficiency gap height is then considered for $-90^\circ \leq \gamma \leq 90^\circ$. For each of these parameter investigations, a Hartmann Number of 200 and Reynolds number of 2000 is considered to maintain consistency with practical limitations, sustain unstable flow behaviour, and meet the validity conditions of the quasi-two-dimensional MHD model proposed by Sommeria and Moreau (1982). A Prandtl number of $Pr = 0.022$ was used throughout, representative of the eutectic alloy GaInSn (Morley et al. 2008).

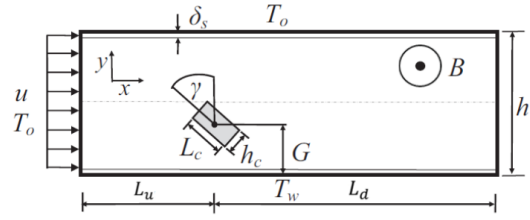


Figure 1: Schematic diagram of the flow configuration and parameters used in the present study. Here, δ_s is the thickness of the sidewall Shercliff layers. Please note that the arrows at the inlet represent the direction of the flow velocity, and is not an accurate representation of the velocity profile shape.

Mathematical Formulation

For sufficiently high Hartmann numbers, and under the assumptions of the Q2D MHD model, the ratio of flow induced to the applied magnetic field, represented by the magnetic Reynolds number Re_m , is very small. Therefore, it is sufficient to consider the applied magnetic field in the out-of-plane direction only. The Q2D model for the present configuration is adapted from that derived by Sommeria and Moreau (1982) and Pothérat et al. (2000). Here, parameter scaling is consistent with that used by Hussam and Sheard (2013), and the reader is asked to refer to this paper for clarification. The dimensionless continuity, momentum, and energy MHD equations can be expressed as

$$\frac{\partial \mathbf{u}}{\partial t} = -(\mathbf{u} \cdot \nabla)\mathbf{u} - \nabla p + \frac{1}{Re} \nabla^2 \mathbf{u} - 2 \frac{L_c^2 Ha}{a^2 Re} \mathbf{u} \quad (1)$$

$$\nabla \cdot \mathbf{u} = 0, \quad (2)$$

$$\frac{\partial T}{\partial t} + (\mathbf{u} \cdot \nabla)T = \frac{1}{Pe} \nabla^2 T, \quad (3)$$

where \mathbf{u} , p and T are the respective velocity, kinematic pressure, and temperature fields in the x - y plane. The Reynolds number Re , Hartmann number Ha and Péclet Pe number are defined as

$$Re = \frac{U_0 L_c}{\nu}, \quad (4)$$

$$H_{L_c} = 2 \left(\frac{L_c}{a}\right)^2 Ha = 2 \left(\frac{L_c}{a}\right)^2 aB\sqrt{(\sigma/\rho\nu)} \quad (5)$$

$$Pe = RePr. \quad (6)$$

Here, L_c , U_0 , ν , σ , B and a are the cylinder length, peak inlet velocity, kinematic viscosity, electric conductivity, applied magnetic field strength and out-of-plane duct height, respectively. The ratio of convective to conductive heat transfer along the heated wall is given by the local Nusselt number

$$Nu_w(x, t) = \frac{h}{T_f - T_w} \frac{\partial T}{\partial y} \Big|_{wall}. \quad (7)$$

The bulk fluid temperature T_f is calculated using the stream-wise velocity component u and temperature distribution

$$T_f(x, t) = \frac{\int_0^h uT dy}{\int_0^h u dy}. \quad (8)$$

A time-averaged Nusselt number for heat transfer through the heated wall of the channel is calculated by first taking the time average of the local Nusselt number ($\overline{Nu_w}$) at each x -station, and then integrating over the length of the heated side-wall using

$$Nu = \frac{1}{L_d} \int_0^{L_d} \overline{Nu_w}(x) dx. \quad (9)$$

The overall efficiency index of the heat transfer augmentation is given as the ratio of the relative heat transfer enhancement to relative pressure drop penalty

with respect to obstacle free reference case under the same flow conditions (denoted by the subscript '0')

$$\eta = \frac{Nu/Nu_0}{\Delta P/\Delta P_0}. \quad (10)$$

Numerical Methodology

A high order spectral element method was employed using an in-house solver to discretise the governing equations. A no-slip boundary condition was applied on all solid surfaces. The channel inlet flow conditions were specified as the analytical solution for fully developed quasi-two-dimensional flow in an empty duct (Poth rat et al. 2000). A constant reference pressure Dirichlet boundary condition and a zero normal velocity gradient Neumann condition were imposed at the duct exit. A high order Neumann pressure gradient was also applied to the other boundaries to maintain third-order time accuracy (Karniadakis et al. 1991). The temperature of the incoming stream and the upper duct side-wall was specified as T_o , and at the heated side-wall as T_w . The cylinder was thermally insulated with a zero normal temperature gradient imposed at its surface. The domain was meshed using a series of macro-elements with internally applied Langrangian polynomial mapping functions. A graded element distribution was employed towards all solid boundaries to resolve regions that experience large flow gradients, such as flow separation at cylinder corners and boundary layers.

The distribution of macro-elements throughout the duct consisted of approximately 30 elements spanning its height and 139 elements (20 upstream and 119 downstream of the cylinder) spanning its length. The thermal and kinematic boundary layers were resolved with a minimum of 7 elements spanning their respective thicknesses. An additional grid resolution study was conducted to ensure adequate spatial and temporal sampling to accurately resolve the dynamics of the flow field. The grid resolution study was conducted by refining the order of the elemental polynomial mapping function over $4 \leq N_p \leq 9$ and measuring the convergence of the domain size and resolution sensitive heat flux, drag coefficient, lift coefficient, and kinetic energy parameters. The $\gamma = 0^\circ$ and $\gamma = 30^\circ$ cases were investigated to represent the extremes of expected flow complexity. For the chosen polynomial order of $N_p = 8$, a convergence of better than 0.3% for all representative parameters was obtained, and this resolution is used hereafter.

Throughout the thermal response plots presented in this paper, the shaded regions about the mean trend line represent the range between the measured global maximum and minimum responses for a given configuration. The additional error bars in these plots illustrate the uncertainty in the thermal response due to long time scale meanderings that may not be fully captured within the recorded time history. This error was estimated by calculating the relative error between two time integration intervals, Δt and $\Delta t/2$.

It should also be noted that for certain orientations, natural convection may be a dominant form of heat transfer under limited conditions (Douset and Poth rat 2008). These effects are not considered in the present investigation. Furthermore, the inclusion of terms characterising the effects of viscous dissipation and Joule heating may be neglected on order of magnitude grounds for the target applications (Hossain 1992).

RESULTS

Gap Height Variation

The effect of gap height variation for an upright cylinder with $Ha = 200$ and $Re = 2000$ on the time-averaged Nusselt number, total pressure drop penalty, and corresponding overall efficiency are illustrated in Figs.2 (a), (b) and (c), respectively. A peak in both pure heat transfer and thermal efficiency of approximately $\eta = 1.6$ occurs when $G/L_c = 1.5$, with a monotonic decrease occurring as the obstacle approaches either the upper or lower walls. As seen for $G/L_c = 1.5$ in the vorticity and temperature contour plots in Fig.3 (b), the vortices shed from the cylinder's lower separation point interact efficiently with the lower wall thermal boundary layer; leading to the transport of large amounts of hot fluid away from the wall without excessive viscous dissipation. This peak efficiency is driven by the radius of the vortical structure being at a near maximum when interacting with the wall-bound fluid.

Increases in thermal enhancement and efficiency over the duct centred configuration ($G/L_c = 2$) is only found for $1.15 \leq G/L_c < 2$. However, all gap heights showed improved thermal efficiency over the empty duct reference case. These findings support those discussed in the introduction with respect to a critical gap height at which heat transfer enhancement can be optimised without detrimental increases in pressure losses above the empty channel reference value of $\Delta P_0 = 1.25$ (Hussam and Sheard 2013).

For $1.85 \leq G/L_c \leq 2.15$, the development of wake symmetry causes the vortex street to advect downstream parallel to the duct walls. This creates a localised region of increased ΔP above the general trend as shown in Fig.2 (b). In regions approaching the upper and lower walls, the highest gradients of Nu , ΔP and η are observed. This is caused by the rapid suppression of near-wall vortices, and in turn, a region of impeded flow near the walls. This is most readily seen in the vorticity and temperature contour plots in Fig.3 (a). For gap heights above the peak efficiency location, vortices are shed increasingly too far from the wall to efficiently entrain the lower thermal boundary layer.

For the centred case shown in Fig.3 (c), periodic shedding of opposite-signed vortices from the cylinder shear layers are observed; leading to the formation of a K rm n vortex street. At this blockage ratio ($\beta = 1/4$), the interaction of the vortex street with the Shercliff layers leads to a substantial loss of wake coherence. This behaviour is amplified when the cylinder is moved closer to either duct wall; where the vortex wake also decays most rapidly downstream. These findings are consistent with those found in Hussam and Sheard (2013) for circular cylinders at $\beta = 0.3$ and $\beta = 0.2$, and confirmed by the breakdown of the two-dimensional K rm n vortex street shown by Frank et al. (2001). As illustrated in Fig.2 (b), mechanical pressure losses also decline rapidly for distances approaching both duct walls as vortex suppression leads to a significant reduction in viscous shear stress. As to be expected due to the omission of natural convection and viscous heating effects in the numerical methodology, the pressure drop distribution is qualitatively symmetric about the duct centreline.

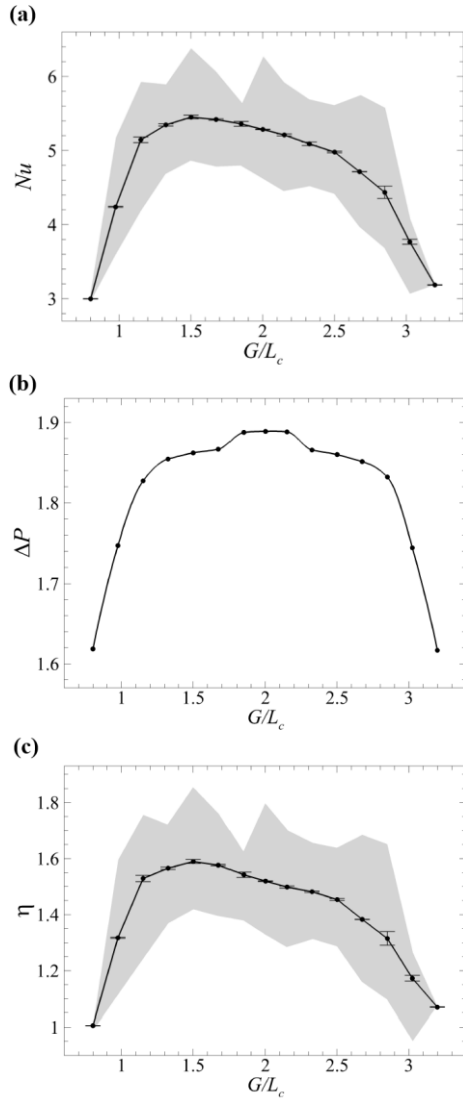


Figure 2: Variation of (a) Nu , (b) ΔP and (c) η for $Re = 2000$, $Ha = 200$ and $0.8 \leq G/L_c \leq 3.2$. The shaded regions on (a) and (c) illustrate the envelope of the temporal variations of the heat transfer due to wake asymmetries. The errors bars provide an uncertainty estimate in the thermal response due to the time interval used to capture the long time-scale meanderings.

The combination of a reduction in pressure losses and the increase in thermal boundary layer entrainment for $1.15 \leq G/L_c \leq 2$, leads to the observed increase in thermal efficiency for these cylinder positions, as shown in Fig.2 (c). The shaded region about the mean trend line depicted in Figs.2 (a) and (c) illustrate the secular variations of these quantities over time due to asymmetry of vortex shedding coupled with the breakdown of the vortex street due to interaction with the Shercliff layers. Points exhibiting a smaller shaded region are closer to time periodicity. The wake asymmetry and breakdown of the vortex street is highlighted by the vorticity contour plots for $G/L_c = 1.5$, and 2 in Figs.3 (b) and (c). It was also observed that wake asymmetry leads to a time-dependent lateral oscillation of the vortex street as it convects downstream. The wake path oscillates between advecting towards the interior of the duct and then to advecting parallel to the duct walls downstream. These results are consistent with observed phenomena in previous studies of impeded MHD flows for similar

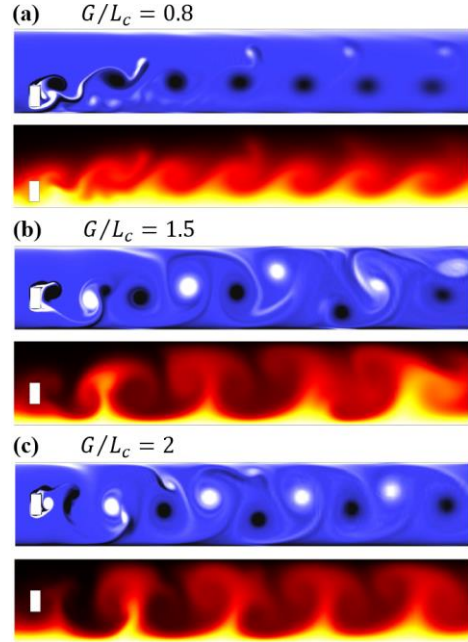


Figure 3: Close-up (40% of the total domain) vorticity (above) and scalar temperature (below) contours for $Re = 2000$ and $Ha = 200$ for gap height ratios (a-c) of $G/L_c = 0.8$, 1.5 and 2, respectively. The vorticity contours range is limited to approximately 10% of the minimum and maximum magnitudes observed. Darker and lighter contours represent positive clockwise rotating and negative counter-clockwise rotating vortices, respectively. The scalar temperature field contours are plotted over a range of $T_o \leq T \leq T_w$ with darker and lighter contours representing colder and hotter fluid, respectively.

interaction parameters and blockage ratios (Mück et al. 2000, Dousset and Pothérat 2012). It has been suggested that the causes of this asymmetry in vortex wakes may be due to slight differences in the shedding frequency of vortices from the cylinder separation points (Dousset and Pothérat 2012). At height ratios where there is large suppression of near wall vortices, such as $G/L_c = 0.8$, the variation in thermal response becomes dominated by the periodic shedding of vortices from the upper cylinder surface, which is highlighted by the smaller shaded regions around these data points. The error bars presented in Figs.2 (a) and (c) remain relatively small for all measured data sets. This implies that the longer time-scale variations of the thermal response is sufficiently captured in the time intervals used for integration.

Incidence angle variation

The effect of incidence angle for $-90^\circ \leq \gamma \leq 90^\circ$ for a cylinder offset from the duct centre-line at $G/L_c = 1.5$ with $Ha = 200$ and $Re = 2000$ on the time-averaged Nusselt number, total pressure drop and the corresponding overall efficiency are illustrated in Figs.4 (a), (b) and (c), respectively. Further improvements in thermal efficiency can be achieved through cylinder inclination over the upright case. A peak of $\eta = 1.7$ was achieved at $\gamma = -37.5^\circ$, which corresponds to an approximate 12% increase over an upright cylinder. Increases in thermal efficiency were also achieved in the regions $-37.5^\circ < \gamma \leq 22.5^\circ$, $-7.5^\circ \leq \gamma < 0^\circ$ and $0^\circ < \gamma \leq 15^\circ$. A minimum thermal efficiency is obtained at $\gamma = -75^\circ$ due to a greater reduction in the rate of change of heat transfer in this region

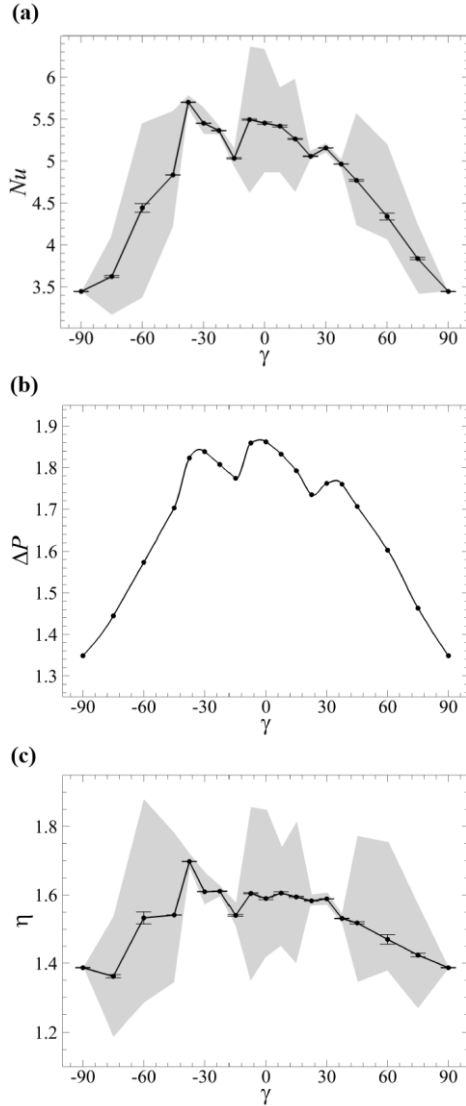


Figure 4: Variation of (a) Nu , (b) ΔP and (c) η for $Re = 2000$, $Ha = 200$, $G/L_c = 1.5$ and $-90^\circ \leq \gamma \leq 90^\circ$. The shaded regions and error bars on (a) and (c) are per Fig.2.

compared to ΔP . Local sharp changes away from the general thermal enhancement trend, such as for $-45^\circ < \gamma \leq 0^\circ$, tend to suggest that the wake dynamics, and in turn the thermal response, are highly sensitive to the coupling of shedding frequency and distance between the cylinder separation points.

Thermal efficiency generally responded better to cylinder inclination than simply offsetting the cylinder. However, these benefits to heat transfer efficiency over an upright cylinder occurred in narrow localised bands of incidence angles. These isolated regions of increased thermal efficiency may be difficult to realise in a practical implementation, where greater engineering tolerances are often required, and deviations from a perfectly uniform upstream flow are likely. A monotonic decrease in both Nu and ΔP is observed for $|\gamma| > 37.5^\circ$ to minima at $|\gamma| = 90^\circ$. Due to the spatial asymmetry at this gap height, the pressure distribution is also asymmetrical about $\gamma = 0^\circ$. Visualisation of instantaneous vorticity and temperature fields from several of the cases from Fig.4 are shown in Fig.5. As highlighted by Fig.5 (c), interaction between

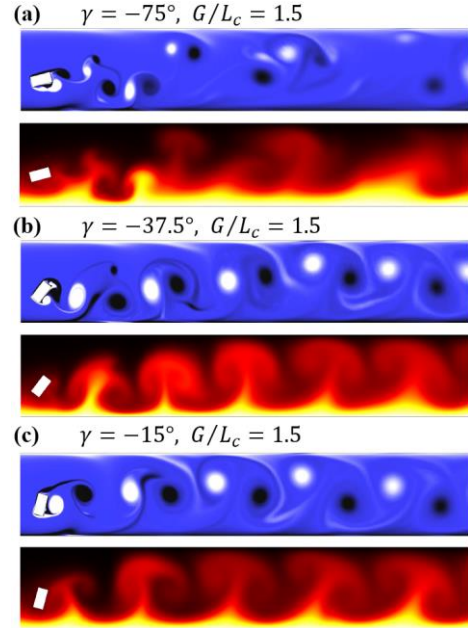


Figure 5: Close up (40% of the total domain) vorticity (above) and scalar temperature (below) contours for $Re = 2000$, $Ha = 200$ and $G/L_c = 1.5$ for incidence angles (a-c) of $\gamma = -75^\circ$, -37.5° , and -15° , respectively. The contour colour map and range are per Fig.3.

lower wall and cylinder shear layers causes the wake to advect downstream near-parallel to the out-of-plane duct walls for $\gamma = -15^\circ$. This behaviour is consistent for other angles in these regions and has the effect of reducing viscous dissipation, and thus leading to the local declines in ΔP observed for $-15^\circ \leq \gamma \leq -7.5^\circ$ and $0^\circ \leq \gamma \leq 22.5^\circ$. It is important to note that a major contributing factor to the overall pressure drop reductions for increased incidence angles is due to the effective reduction in blockage ratio.

As highlighted by the shaded regions on Figs.4 (a) and (c), angles in the region $-45^\circ \leq \gamma \leq -15^\circ$ and $22.5^\circ \leq \gamma \leq 45^\circ$ show small secular variations of Nu over time. In this region the heat transfer enhancement response is in lock-step with the periodic shedding of the vortices from the vortex promoter. For these incidence angles, the thermal response is not heavily affected by the lateral wake oscillations or the loss of wake coherence due to interactions with the Shercliff layers. This is nicely illustrated by the clear periodic plumes of hot fluid carried downstream coinciding with the advection of the vortex structures shown in Figs.5 (b) and (c).

To help quantify this behaviour, Fig.6 presents the scaled mean Fourier spectra for the time-dependent Nusselt number for both the $\gamma = -37.5^\circ$ and $\gamma = 0^\circ$ cases. Consistent with the $\gamma = -37.5^\circ$ uniform vorticity and scalar structures seen in Fig.5 (b), the corresponding Fourier spectrum exhibits strong narrow peaks and harmonics corresponding to the highly periodic and uniform heat transfer response. In contrast, the $\gamma = 0^\circ$ case shows a significant increase in spectrum energy as $\omega \rightarrow 0$, coupled with a considerable widening of the peaks and dispersion of energy across the spectrum. This is consistent with the comparable increase in wake disorder and loss of coherent thermal boundary layer entrainment seen in the vorticity and temperature contour plots in Fig.5 (b).

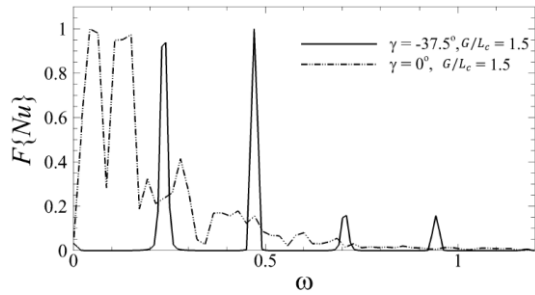


Figure 6: Fourier spectra of the time-dependent Nusselt number ($F\{Nu\}$) for $\gamma = 0^\circ$ and -37.5° at $G/L_c = 1.5$, $Ha = 200$ and $Re = 2000$.

The breakdown of the heat transport structures coinciding with the loss of periodicity of the vortices help to explain the observed differences in the low frequency variations of the thermal response over time for such cases. The relatively small error estimates shown in Figs. 4 (a) and (c) suggest that the longer time-scale variations of the thermal response is again sufficiently captured in the time intervals used for integration.

As illustrated via the vorticity and temperature contours in Fig.5 (c), the localised decrease in the general Nu trend around $\gamma = -15^\circ$ is due to the shearing of the vortex pair towards the upper wall immediately after forming. For this case, the wake does not interact strongly with the lower wall until further downstream, where much of the rotational energy transporting hot fluid upwards has already been dissipated. For the peak efficiency case, shown in Fig.5 (b), the opposite behaviour is now observed. The vortex pair advect downward towards the lower wall while the angular momentum is at a near maximum; thus, effectively sweeping hot fluid away from the lower wall at increased rates. Furthermore, the vortices are shed at such an angle as to maximise the interaction time with the lower wall thermal boundary layer as they advect downstream. In contrast, for $37.5^\circ \leq |\gamma| \leq 75^\circ$ we see that the merging of the vortex pair aft of the obstacle essentially cancel their respective angular momenta. This in turn leads to a chaotic disordered wake, as shown in as highlighted by Fig.5 (a), which is detrimental to heat transport within the channel.

CONCLUSION

The present study numerically investigated the heat transfer and pressure drop characteristics of confined liquid metal ($Pr = 0.022$) flow under a strong axial magnetic field past a rectangular cylinder at varying gap height and incidence angle. The effect of gap height ratio G/L_c of a single upright cylinder for $0.8 \leq G/L_c \leq 3.2$ on heat transfer efficiency was firstly considered. This was followed by an investigation on the effect of cylinder incidence angle γ on heat transfer efficiency for at the optimal efficiency gap height. For each of these investigations, a Hartmann number of $Ha = 200$ and a Reynolds number $Re = 2000$ were employed. It was found that the thermal efficiency can be improved by offsetting the cylinder at gap height ratios $1.15 \leq G/L_c < 2$, with a peak occurring at $G/L_c = 1.5$. Additional benefits in thermal efficiency could also be achieved at $G/L_c = 1.5$ by inclining the cylinder at angles $-37.5^\circ < \gamma \leq 22.5^\circ$, $-7.5^\circ \leq \gamma < 0^\circ$ and $0^\circ < \gamma \leq 15^\circ$, with a peak efficiency occurring at $\gamma = -37.5^\circ$. It was also found that increases in mechanical penalties and heat transfer are not always positively correlated.

ACKNOWLEDGEMENTS

O. G. W. C was supported by an Engineering Research Living Allowance (ERLA) scholarship from the Faculty of Engineering, Monash University. This research was supported by Discovery Grants DP120100153 and DP150102920 from the Australian Research Council, and was undertaken with the assistance of resources from the National Computational Infrastructure (NCI), which is supported by the Australian Government.

REFERENCES

- BRANOVER, H., et al. (1995). "Use of turbulence modification for heat transfer enhancement in liquid metal blankets." *Fusion Engineering and Design* **27**(0): 719-724.
- CHATTERJEE, D. and GUPTA, S. K. (2015). "MHD flow and heat transfer behind a square cylinder in a duct under strong axial magnetic field." *International Journal of Heat and Mass Transfer* **88**: 1-13.
- DOUSSET, V. and A. POTHÉRAT (2008). "Numerical simulations of a cylinder wake under a strong axial magnetic field." *Physics of Fluids (1994-present)* **20**(1).
- DOUSSET, V. and A. POTHÉRAT (2012). "Characterization of the flow past a truncated square cylinder in a duct under a spanwise magnetic field." *Journal of Fluid Mechanics* **691**: 341-367.
- FRANK, M., et al. (2001). "Visual analysis of two-dimensional magnetohydrodynamics." *Physics of Fluids (1994-present)* **13**(8): 2287-2295.
- HOSSAIN, M. A. (1992). "Viscous and Joule heating effects on MHD-free convection flow with variable plate temperature." *International Journal of Heat and Mass Transfer* **35**(12): 3485-3487.
- HUSSAM, W. K. and G. J. SHEARD (2013). "Heat transfer in a high Hartmann number MHD duct flow with a circular cylinder placed near the heated side-wall." *International Journal of Heat and Mass Transfer* **67**(0): 944-954.
- HUSSAM, W. K., et al. (2012). "Optimal transient disturbances behind a circular cylinder in a quasi-two-dimensional magnetohydrodynamic duct flow." *Physics of Fluids (1994-present)* **24**(2).
- KANARIS, N., et al. (2013). "Three-dimensional numerical simulations of magnetohydrodynamic flow around a confined circular cylinder under low, moderate, and strong magnetic fields." *Physics of Fluids (1994-present)* **25**(7).
- KARNIADAKIS, G. E., et al. (1991). "High-order splitting methods for the incompressible Navier-Stokes equations." *Journal of Computational Physics* **97**(2): 414-443.
- MEIS, M., et al. (2010). "Heat transfer enhancement in micro-channels caused by vortex promoters." *International Journal of Heat and Mass Transfer* **53**(1-3): 29-40.
- MORLEY, N. B., et al. (2008). "GaInSn usage in the research laboratory." *Review of Scientific Instruments* **79**(5): 056107.
- MÜCK, B., et al. (2000). "Three-dimensional MHD flows in rectangular ducts with internal obstacles." *Journal of Fluid Mechanics* **418**: 265-295.
- POTHÉRAT, A., et al. (2000). "An effective two-dimensional model for MHD flows with transverse magnetic field." *Journal of Fluid Mechanics* **424**: 75-100.
- SOMMERIA, J. and R. MOREAU (1982). "Why, how, and when, MHD turbulence becomes two-dimensional." *Journal of Fluid Mechanics* **118**: 507-518.
- YOON, H. S., et al. (2004). "A numerical study on the fluid flow and heat transfer around a circular cylinder in an aligned magnetic field." *International Journal of Heat and Mass Transfer* **47**(19-20): 4075-4087.